Communication in Physical Sciences, 2024, 11(4): 767-784

The Geochemistry and Petrogenesis of the Iron-Bearing Sediments of Mfamosing, Southeastern (SE), Nigeria: Evidence from Major Oxides and Its Implication for Industrial Utilization

Benjamin Odey Omang *, Temple Okah Arikpo, Eyong Gods'will Abam, Asinya Enah Asinya, Godwin Terwase Kave and Anthony Adesoji Onasanwo
Received: 12 July 2024/Accepted: 20 Augus 2024/Published: 26 August 2024

Abstract: *Iron ore, a critical resource for global industrial activities, plays a pivotal role in driving economic development and sustaining essential sectors such as construction, manufacturing, and infrastructure. Nigeria is endowed with substantial iron ore reserves, including the Mfamosing area, which has recently garnered attention for its untapped potential. However, limited comprehensive studies hinder a clear understanding of the iron ore occurrences and their industrial viability. This study addresses this gap by investigating the geochemistry of the iron-bearing metasediments in the Mfamosing area, utilizing X-ray fluorescence (XRF) to analyze major oxides. Field and laboratory studies were conducted, involving the collection of twenty-five (25) sediment samples from the Mfamosing area and subsequent XRF analysis. The results revealed a high content of Fe_2O_3 (hematite) in the range of 62.64–80.45 wt.%, indicating the dominance of iron-rich minerals. The presence of SiO_2, Al_2O_3, and other oxides suggests potential gangue minerals and aids in understanding the ore's composition. The petrogenesis study compares the geochemical characteristics of the Mfamosing iron ore with other iron-bearing formations globally. The findings indicate a sedimentary origin, with hydrothermal influence evidenced by Fe/Al and Fe/Si ratios. The low concentration of detrital materials further supports a primarily seawater-derived iron source. The iron ore has low concentrations of deleterious elements. Classification based on Fe_2O_3 content places most samples in the high-grade category, making them suitable as a primary raw material for steel production. Comparisons with other iron formations in Nigeria and worldwide affirm the Mfamosing iron ore's competitiveness on a global scale.*

Keywords: *Geochemistry Petrogenesis, Iron ore , Mfamosing, Calabar Flank.*

Benjamin Odey Omang
Department of Geology, University of Calabar, P.M.B 1115, Calabar, Cross River State, Nigeria
Email: odeyben@gmail.com
Orcid **id:** 0000-0001-9196-3109

Temple Okah Arikpo
Department of Geology, University of Calabar, P.M.B 1115, Calabar, Cross River State, Nigeria
Email: arikpotemple@gmail.com
Orcid **id**: 0009-0002-9425-0125

Eyong Gods'will Abam
Department of Geology, University of Calabar, P.M.B 1115, Calabar, Cross River State, Nigeria
Email: godswill_eyong@yahoo.com

Godwin Terwase Kave
Department of Geology, University of Calabar, P.M.B 1115, Calabar, Cross River State, Nigeria
Email: gkaves@yahoo.com

Asinya Enah Asinya
Department of Geology, University of Calabar, P.M.B 1115, Calabar, Cross River State, Nigeria
Email: asinyaenya@gmail.com

Anthony Adesoji Onasanwo
Department of Geology, University of Calabar, P.M.B 1115, Calabar, Cross River State, Nigeria
Email: adsojt@gmail.com

1.0 Introduction

Iron formations represent significant stratigraphic units primarily consisting of iron-rich chemical sedimentary rock often

referred to as ironstone (Kimberley, 1978a). They are mostly chemical sedimentary rock with over 15% Fe (Bekkar *et al*., 2010; Cox *et al*., 2013; Kimberley, 1078; Marion *et al*., 2021; Planavsky, 1978; Marion *et al*., 2021; Planavsky, 2012; Posth *et al*., 2013;Yang *et al*., 2016). fa

The intricate geological processes leading to the genesis of iron formations result in diverse deposits (Bekker *et al.,* 2014; Konhauser *et al.,* 2017; Zhang *et al.,* 2014). These include Banded Iron Formations (BIFs). This is a specific type of iron formation, which are sedimentary rocks recognized for their alternating layers of iron-rich minerals and silica-rich minerals, likely formed through the precipitation of iron and silica from ancient seawater in shallow marine environments (Clout & Simonson, 2005; Hagemann *et al.,* 2016; Nanda & Beura, 2021; Sun & Li, 2017; Taner & Chemam, 2015; Yin *et al.,* 2023). Magnetite deposits, characterized by the prevalence of the mineral magnetite (Fe_3O_4), often originate from magmatic processes or the concentration of iron by hydrothermal fluids (Moisescu *et al.,* 2014). Hematite deposits, primarily composed of hematite (Fe_2O_3), can form through various mechanisms, including alteration, hydrothermal precipitation, and metamorphism *(*Minitti *et al., 2005*; Öztürk *et al.,* 2016; Xing *et al.,* 2021). Weathered iron ore deposits, like goethite (FeO (OH)) and limonite ($FeO(OH)\cdot nH_2O$), result from the weathering of primary iron minerals under atmospheric conditions(Santoro *et al.,* 2022). Kiruna-type deposits are extensive, high-grade iron ore deposits associated with intrusive magmatic rocks, while Superior-type iron deposits are linked to volcanic and sedimentary rocks in greenstone belts, formed through volcanic and hydrothermal processes. Iron ore deposits result from various geological processes, such as sedimentation, magmatism, and metamorphism, with dominant iron minerals including hematite, magnetite, limonite, and siderite (Rojas *et al.,* 2018). The mineral composition and textural features depend on the formation environment and subsequent alterations. Iron ore deposits often contain associated elements like manganese, titanium, phosphorus, and sulfur, impacting quality and processing requirements*(*Liu *et al., 2019;* Ochromowicz *et al.,* 2021).

Trace elements like arsenic, cadmium, and lead can pose environmental concerns, necessitating additional purification steps (Vishiti *et al*.,2004; Nkuna *et al.,* 2022). Four types of iron formations are classified based on lithology, composition, associated rocks, and depositional environment: (i) Clinton type and Minette type consist of grained iron formations (GIFs), featuring a granular texture and the absence of laminations/banding; (ii) Algoma-type and Superior-type, known as banded iron formations (BIFs), are mainly banded cherty rocks and contribute significantly to global iron production (Jean-Lavenir *et al.,* 2023). The principal difference lies in the depositional environment, with Algoma-type formations deposited as chemical sediments along with other sedimentary rocks and volcanic material, while Superior-type formations were chemically precipitated on marine continental shelves and in shallow basins (Gourcerol *et al.,* 2016; Li *et al.,* 2022). Algoma- and Superior-type formations share similar mineralogy, with stilpnomelane present only in Algoma-type, indicating potential contamination with volcaniclastic detritus(Wang *et al.,* 2014).

Iron ore serves as a fundamental raw material with diverse applications across various industries. Primarily crucial for steel production, it undergoes smelting in blast furnaces to yield pig iron, the principal ingredient in steel manufacturing. The construction industry heavily relies on steel derived from iron ore for structural components, beams, and reinforcing bars in projects such as bridges and buildings. In transportation, iron and steel find applications in vehicle construction, contributing to the automotive sector, as well as in the production of railways, ships, and aeroplanes. The machinery and equipment manufacturing sector also depends on iron and steel for the fabrication of industrial

machinery and tools. Steel plays a vital role in energy infrastructure, supporting projects like wind turbines, power plants, and oil and gas pipelines. Consumer goods, ranging from appliances to furniture, utilize steel due to its strength and durability. Additionally, iron and steel have applications in containers and packaging, medicine (as supplements and in medical imaging), water treatment processes, fertilizers, and even in the art and decorative industries (Das *et al.,* 2007; Reddy *et al.,* 2019; Thombare *et al.,* 2016). With its versatility, iron ore remains a cornerstone in the global economy, impacting numerous facets of daily life and industrial processes. The rapid economic growth in certain countries like India and China has led to an increased demand for steel in the world market. Consequently, there has been a surge in Fe ore exploration to meet this demand. The banded iron formation (BIF) from the Archaean Ntem Complex (Congo Craton) in the Meyomessi Area, Southern Cameroon, as studied by Sylvestre *et al.* (2018), reveals that iron and silica are the main constituents. The total iron (TFe) contents range from 48.71 to 65.32 wt% (average of 53.29 wt %), making it relatively high-grade or medium-grade iron ore by global standards, suitable for industrial applications (Ndime *et al.,* 2018). The results of BIF from the Mamelles iron ore deposit in the Nyong unit, South-West Cameroon, as investigated by Teutsong *et al*. (2020), show that Fe_2O_3, SiO_2, and Al_2O_3 ranged from 72 to 76.40 wt%, 16.70 to 18.35 wt%, and 2.80 to 5.43 wt%, respectively. TiO_2 varies from 0.14 to 0.18 wt%, and P_2O_5 from 0.13 to 0.34 wt%. This study indicates that the Mamelles deposit contains medium-grade iron ores with acceptable contents in contaminants (Teutsong *et al.,* 2021). Studies reveal that Itakpe ore is richer in iron than either the Agbaja or the Corby ores. Itakpe is a fairly high-grade, acidic (or siliceous) ore, whereas Agbaja is a low-grade, high-phosphorus, acidic ore, and Corby is a low-grade, high-phosphorus ore that is basic (or calcareous) due to its high calcite content (Adedeji & Sale, 1984). The Maru BIF shows Fe_2O_3 ranging from 44.07 to 58.41%, SiO_2 from 24.74 to 42.67%, with relatively high values of Al_2O_3 (2.00 to 8.97%) and MnO (2.29 to 9.37%) (Adekoya, 1998). The Maru BIF is low to moderate grade and will require advanced techniques for processing.

Nigeria is endowed with substantial iron ore reserves, including the Mfamosing area, which has recently garnered attention for its untapped potential. However, limited comprehensive studies hinder a clear understanding of the iron ore occurrences and their industrial viability. This study addresses this gap by investigating the geochemistry of the iron-bearing metasediments in the Mfamosing area.

1.1 Location of the study area

The study was carried out within the Mfamosing areas, between latitude N 5° 5' 00" to N 5° 10' 0" and longitude E8° 24' 0" to E8° 25' 0". It is situated in the South Eastern region of Nigeria (Fig. 1). The area is about 30km away from the main settlement, and it is accessed by the use of motorcycles. These areas have been identified as holding significant iron ore occurrences hosted within the Mfamosing formation of the Calabar Flank.

1.2. Geologic settings

The earliest investigations into the geology of the Calabar Flank were conducted by Reyment (1955) and Dessauvagie (1965). They established the basin's biostratigraphic context. Although Reyment (1955) initially regarded it as part of the Benue Trough, Murat (1972) later believed that the Calabar Flank experienced a distinct phase of tectonism and stratigraphic evolution compared to the adjacent Anambra Basin and the lower Benue Trough, thereby categorizing it as a separate basin (Ekwok *et al.,* 2021; Okon *et al.,* 2022). Nyong and Ramanathan (1985) defined the Calabar Flank as the easternmost segment of the Gulf of Guinea, which constitutes part of the Nigerian continental margin. This area is sandwiched between the Cameroon volcanic line to the east, the Ikpe platform to the west, and the Oban Massif and Calabar hinge line to the north and south, respectively.

The Calabar Flank is a relatively compact Nigerian sedimentary basin which lies along the fringes of the Gulf of Guinea. A significant divergence between the Calabar Flank and the southern Benue Trough originates from the initial rifting of the southern Nigerian margin. This event gave rise to two primary sets of faults, notably the NE-SW and NW-SW trending fault sets that characterize the Benue Trough and the Calabar Flank respectively (Murat, 1972). Within this context, Murat (1972) identifies the tectonic components of the Calabar Flank as including the Ikang Trough and the Ituk High, which represented a mobile depression and a stable mobile submarine ridge. They further postulated that the Calabar Flank is underlain by horsts and graben structures. Sedimentary processes within the Calabar Flank commenced with the deposition of fluvio-deltaic clastics known as the Awi Sandstone, likely of Aptian age, overlying the Precambrian crystalline basement complex known as the Oban Massif. This phase was succeeded by a mid-Albian marine transgression, leading to the accumulation of the Mfamosing Limestone. This limestone was primarily deposited on horst structures and relatively stable platforms. (Ekwok *et al.,* 2019; Adamu *et al.,* 2021). Above the Mfamosing Limestone is a substantial sequence of black to grey shale known as the Ekenkpon Formation (Petters & Reijers, 1987). This formation displays minor occurrences of marls, calcareous mudstone, and oyster beds deposited during the late Cenomanian-Turonian. (Petters & Reijers, 1987).

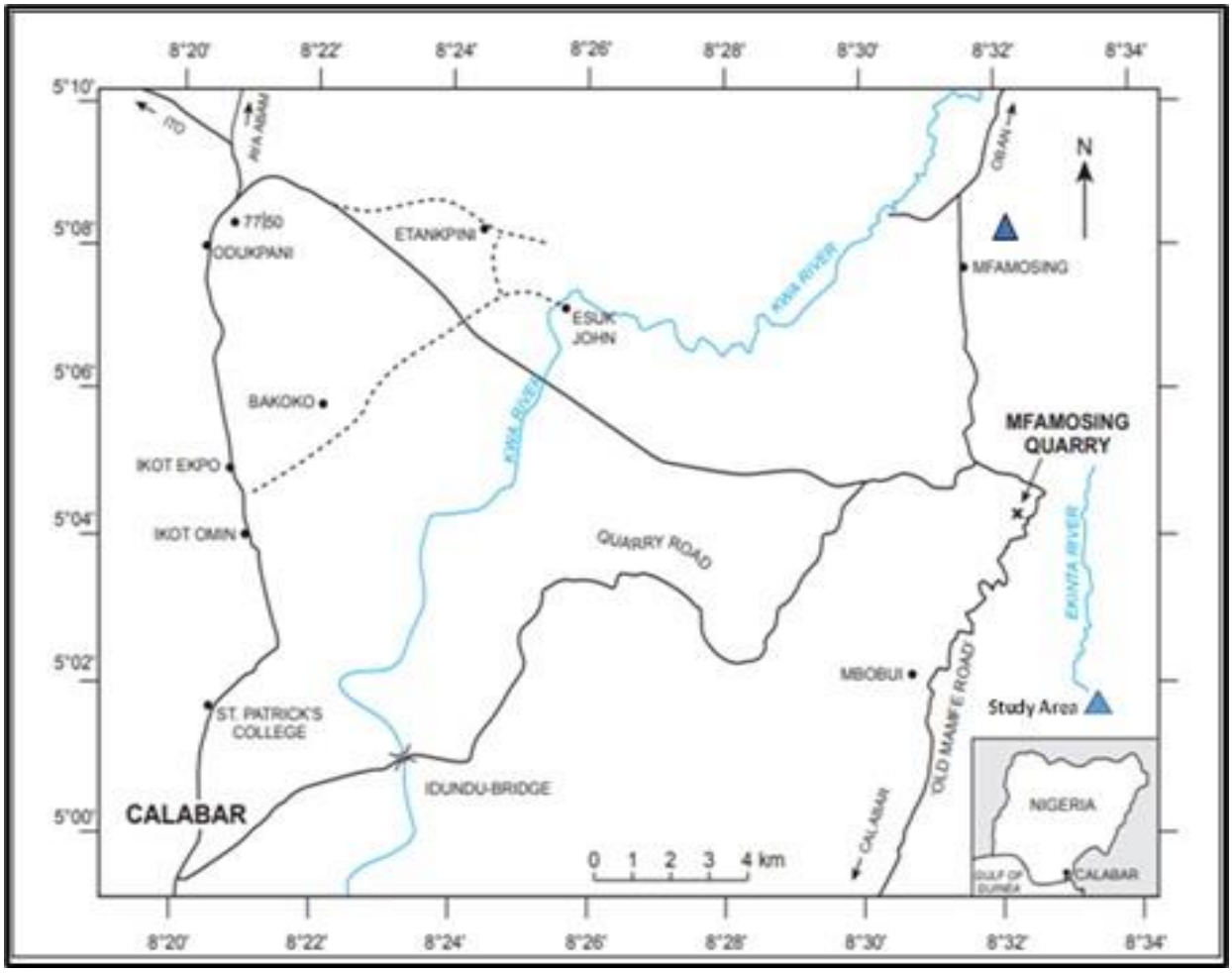

Fig. 1. Map of southeastern Nigeria showing the location of the study area (William *et al*. 2019)

Ukpong and Ekhalialu (2015) further confirm this age using foraminifera and palynomorph analysis. The Ekenkpon Shale is overlain by a thick marl unit referred to as the New Netim Marl. This unit is characterized by nodules and shale at its base, with intermittent thin layers of shale in its upper portion (Harry, 2022). Foraminiferal analysis indicates an early Coniacian age for the New Netim Marl (Anoh & Petters, 2014). Following an unconformity, the carbonaceous dark grey shale of the Nkporo Formation overlays the New Netim Marl. This shale unit was deposited during the late Campanian-Maastrichtian interval and serves as the uppermost layer of the Cretaceous sequence within the Calabar Flank. Finally, the Nkporo Shale sequence is succeeded by a pebbly sandstone unit representing the Tertiary Benin Formation as seen in Fig. 2 (Edegbai *et al.,* 2019; Omietimi *et al.,* 2022; Uzoegbu *et al.,* 2023; Omang *et al.,* 2023; Omang *et al.,* 2023)

AGE	LITHOLOGY		DESCRIPTION
Recent Eocene -	Benin Formation		Loose sands, pebbly and arkosic
Maastrichtian L. Campanian -	Nkporo Shale		Dark grey, very fissile carbonaceous shale with gypsum bands and some calcareous nodules
Santonian	Santonian Deformation		Santonian deformational episode characterized by period of folding of pre-existing rocks and erosion and/or non deposition.
Coniacian	ODUKPANI GROUP	New Netim Marl	Dark grey massive marls intercalating with flaggy, calcareous grey shale with thalassinoides structures
Turonian		Ekenkpon Shale	Grey fissile shale with thin bands of calcareous nodules, limestone and mudstone units. Abundant shell fragments, keeled ammonite, juvenile
Cenomanian		Un-named Shale	Dark gray shale, highly fissile and separated by the upper shale unit by a regressive mudstone
Mid - Albian		Mfamosing Limestone	White to light grey limestone, stromatolitic at the base, with abundant fossils (gastropods, corals, shell fragments)
Neocomian - Aptian	Awi Formation		Reddish brown, coarse to medium grained arkosic sandstone. Pebbly at the base and exhibit fining upward succession in cycles, graded bedding.
Precambrian	Precambrian Basement Complex		Southeastern Basement Complex – Oban Massif composed predominantly of granite gneisses, granites and granodiorites.

Fig. 2. Stratigraphic chart of the Calabar Flank (Modified after Petters et al., 2014)

2.0 Materials and Methods

The methodology encompassed comprehensive fieldwork, alongside geochemical analyses of rock samples. During the field study, twenty-five (25) rock samples weighing 5 to 10 kg before removing the weathered phases were meticulously collected from various rock outcrops within Mfamosing. Collected samples were cleansed to remove visible allogenic material and observed weathered phases before transportation to the laboratory. All the samples were subjected to geochemical analysis. For the geochemical analysis, approximately 2 kg of each representative rock sample was fragmented into thumb-nail-sized pieces using a hardened steel hammer. These pieces were then divided, with one part reserved for reference purposes and the other crushed and ground to attain a particle size finer than -60 mesh, facilitated by a "jaw-crusher". Each sample was powdered to -200 mesh and homogenized, exercising utmost care to prevent cross-contamination between samples. The homogenized ore samples were then quartered for subsequent analyses. Major element composition in the studied rocks was determined using the XRF technique.

Dehydrated powdered samples were fused with lithium tetraborate in a platinum alloy crucible at 1100°C to produce fused beads for analysis. The XRF raw data were corrected using "alpha factors" for inter-element correction. Major elements like Silica (SiO_2), Aluminum oxide (Al_2O_3), Iron (III) oxide (Fe_2O_3), Manganese oxide (MnO), Magnesium oxide (MgO), Calcium oxide

(CaO), Sodium oxide (Na_2O), Potassium oxide (K_2O), and Sulphur oxide (SO_2) were measured as oxides. Calibration was achieved using certified international reference rock materials.

3.0 Results and Discussion

The result of the geochemical analysis of the Mfamosing iron formation is presented in Table 1.

3.1. Major Oxide Geochemistry

The predominant bulk chemical composition of the analyzed sample reveals a substantial abundance of Fe_2O_3 (hematite), ranging from 62.64 to 80.45 wt.% and averaging at 70.98 wt.%. This signifies a notably high iron content, characteristic of hematite-rich deposits. The concurrent presence of SiO_2, within the range of 5.49 to 11.58 wt.%, suggests the occurrence of quartz—a common gangue mineral in iron ores known for its association with hematite. Additionally, the presence of Al_2O_3 (3.53 to 7.26 wt.%) points towards the potential existence of mineral phases such as clays or aluminosilicates, acting as gangue minerals (Hussin *et al*., 2018). The observed low concentrations of oxides like MgO, CaO, MnO, and TiO_2 in the sample suggest a minimal influence of contamination from other rock types/minerals like carbonate rocks, apatite, pyroxene or hydrothermal alteration processes (Omotunde, 2020; Omang *et al*., 2023; Vural, 2023). This emphasizes the purity and distinctiveness of the analyzed material.

An intriguing aspect arises from the weak negative correlation observed between Fe_2O_3 and SiO_2 (r = -0.3), Al_2O_3 (r = -0.06), and CaO (r = -0.39), as indicated in Table 2. This correlation implies an inverse relationship between these oxides and iron minerals. Such a trend suggests a possible chemical precipitation mechanism during the formation of iron ores, wherein iron oxides may have replaced or excluded SiO_2, Al_2O_3, and CaO (Fiege, 2019; Madondo *et al.,* 2021). This phenomenon could offer valuable insights into the geological processes that led to the ore's composition and formation. Comparative analysis with other iron formations, namely Gangfelum BIF, Maru BIF, Muro BIF, and Kankun BIF (detailed in Table 3), highlights the distinctive nature of the analyzed sample (Bolarinwa, 2017). Specifically, the Fe_2O_3 content in the studied samples surpasses that of the mentioned iron formations, underlining its unique composition within the broader geological context. This disparity in iron content further accentuates the significance and potential economic value of the analyzed deposit.

3.2. Petrogenesis

The SiO_2-Al_2O_3-FeO ternary diagram, based on the classification system proposed by Govett *et al*. 1966 (Fig. 3), provides valuable insights into the age and genesis of the Mfamosing iron ore. The positioning of the ore in the diagram strongly indicates a post-Precambrian age, aligning with the observed characteristics of the deposit (Bafon *et al.*, 2023).

The identified weak negative correlation between Fe_2O_3 and SiO_2 (r = -0.3) aligns well with a sedimentary origin for the Mfamosing iron ore, as illustrated in Fig. 4.

In sedimentary settings, such correlations often suggest a transformation process where iron minerals precipitate, replacing silicate minerals like quartz. This interpretation adds depth to the understanding of the ore formation mechanism, with sedimentary processes playing a significant role in the composition of the deposit. The distinctive composition of the Mfamosing iron ore, characterized by extremely low concentrations of other oxides and the dominance of Fe_2O_3, which is in line with the attributes commonly associated with sedimentary iron ores

This is in contrast to magmatic iron ores, which typically exhibit a broader range of oxide compositions, including various metal oxides (Skirrow, 2022). The high Fe/Al (19.26) and Fe/Si (14.46) ratios, in comparison to the Si/Al ratio (1.37), strongly suggest a notable hydrothermal influence in the ore formation process, as indicated by (Hatton & Davidson, 2004; Jansson & Allen, 2011). These ratios serve as robust indicators of the involvement of hydrothermal fluids,

potentially contributing to the enrichment of iron in the ore.

Table 1: Geochemical Characteristics of Mfamosing Iron Ore

Sample ID	M14	M15	M16	M17	M18	M19	M20	M21	M22	M23	M24	M25	MEAN	Range
SiO_2	5.68	6.83	7.91	6.03	6.65	11.58	8.15	8.83	8.05	10.26	9.25	7.17	7.70	5.49-11.58
Al_2O_3	3.53	5.32	5.68	4.41	5.05	7.26	5.33	5.62	5.12	4.93	5.12	4.45	5.01	3.53-7.26
Fe_2O_3	72.20	70.10	73.12	71.79	72.35	70.32	73.15	70.60	71.44	70.19	73.14	74.75	70.98	62.64-80.05
CaO	0.01	0.05	0.10	0.02	0.12	0.43	0.11	0.07	0.09	0.20	0.13	0.01	0.10	0.00-0.43
MgO	0.00	0.00	0.00	0.00	0.00	0.00	0.00	0.00	0.00	0.00	0.00	0.00	0.00	0.00-0.00
SO_2	0.00	0.00	0.00	0.00	0.00	0.00	0.00	0.00	0.00	0.00	0.00	0.00	0.00	0.00-0.00
K_2O	0.00	0.03	0.06	0.03	0.00	0.05	0.02	0.07	0.07	0.08	0.08	0.05	0.05	0.00-0.11
Na_2O	0.02	0.01	0.02	0.00	0.00	0.00	0.00	0.00	0.00	0.00	0.00	0.00	0.00	0.00-0.03
TiO_2	0.00	0.00	0.00	0.00	0.00	0.00	0.00	0.00	0.00	0.00	0.00	0.00	0.00	0.00-0.00
Mn_2O	0.00	0.00	0.00	0.00	0.00	0.00	0.00	0.00	0.00	0.00	0.00	0.00	0.00	0.00-0.00
P_2O_5	0.00	0.00	0.00	0.00	0.00	0.00	0.00	0.00	0.00	0.00	0.00	0.00	0.00	0.00-0.00
LOI	13.52	13.43	13.24	14.25	12.90	12.30	12.48	13.00	12.85	14.07	12.01	13.98	13.52	12.01-15.70
Total	94.96	94.90	99.95	98.54	97.06	99.92	99.23	98.18	97.61	99.74	99.73	100.00	-	-
Si/Al	1.42	1.13	1.23	1.21	1.16	1.41	1.35	1.39	1.39	1.84	1.60	1.42	1.37	1.07-2.01
Fe/Al	27.08	17.45	17.05	21.56	18.97	12.83	18.17	16.63	18.48	18.85	18.92	22.24	19.26	

Table 2. Pearson's correlation matrix for major element oxides in the study area

	SiO2	*Al2O3*	*Fe2O3*	*CaO*	*K2O*	*Na2O*	*LOI*
SiO2	1						
Al2O3	0.528194	1					
Fe2O3	-0.29988	-0.05919	1				
CaO	0.806823	0.615551	-0.38987	1			
K2O	0.3516	0.160537	-0.53162	0.34558	1		
Na2O	-0.39446	-0.33234	0.341497	-0.34252	-0.26954	1	
LOI	-0.54975	-0.4018	0.428354	-0.56692	-0.30244	0.622269	1

Table 3. Comparison of the study area major oxides (wt-%) with BIF types in Nigeria (Anthony, 2018)

Location	This study	Gangfelum BIF	Maru BIF	Muro BIF	Kakun BIF
SiO_2	7.70	41.98	34.35	57.66	20.17
TiO_2	0.00	0.37	0.16	0.02	1.74
Al_2O_3	5.01	1.41	4.25	0.28	8.12
Fe_2O_3(t)	70.98	53.91	54.3	42.02	56.8
MnO	0.00	0.09	4.83	0.06	0.07
MgO	0.00	0.02	0.13	0.01	3.58
CaO	0.10	0.05	0.11	0.02	6.68
Na_2O	0.00	0.18	0.01	0.01	1.1
K_2O	0.05	0.44	0.65	0.02	0.77
P_2O_5	0.00	<0.01	0.09	0.05	0.27

The plotting of the iron ore samples within the deep-sea pelagic sediment field in the SiO_2-Al_2O_3 discrimination plots, following the classification by Bostrom *et al*., 1973 (Fig. 5), further supports the hypothesis that the iron in the Mfamosing deposit primarily originated from dissolved iron in seawater (Tchouakui *et al.,* 2022). This interpretation implies a limited input of detrital materials such as quartz and aluminium-rich clays, emphasizing the marine influence on the ore's composition. The low Al_2O_3+TiO_2 value (5.01 wt.%), in contrast to the Fe/Al and Fe/Si ratios, serves as additional confirmation of the reduced input of detrital materials, highlighting the purity of the iron ore. Furthermore, the role of hydrothermal fluids in ore formation is evident in Fig. 6, illustrating the potential interaction of hot, mineral-rich fluids from hydrothermal vents with seawater, leading to the precipitation of iron oxides. This multifaceted approach to analyzing the Mfamosing iron ore provides a comprehensive understanding of its genesis, age, and the geological processes that shaped its unique composition.

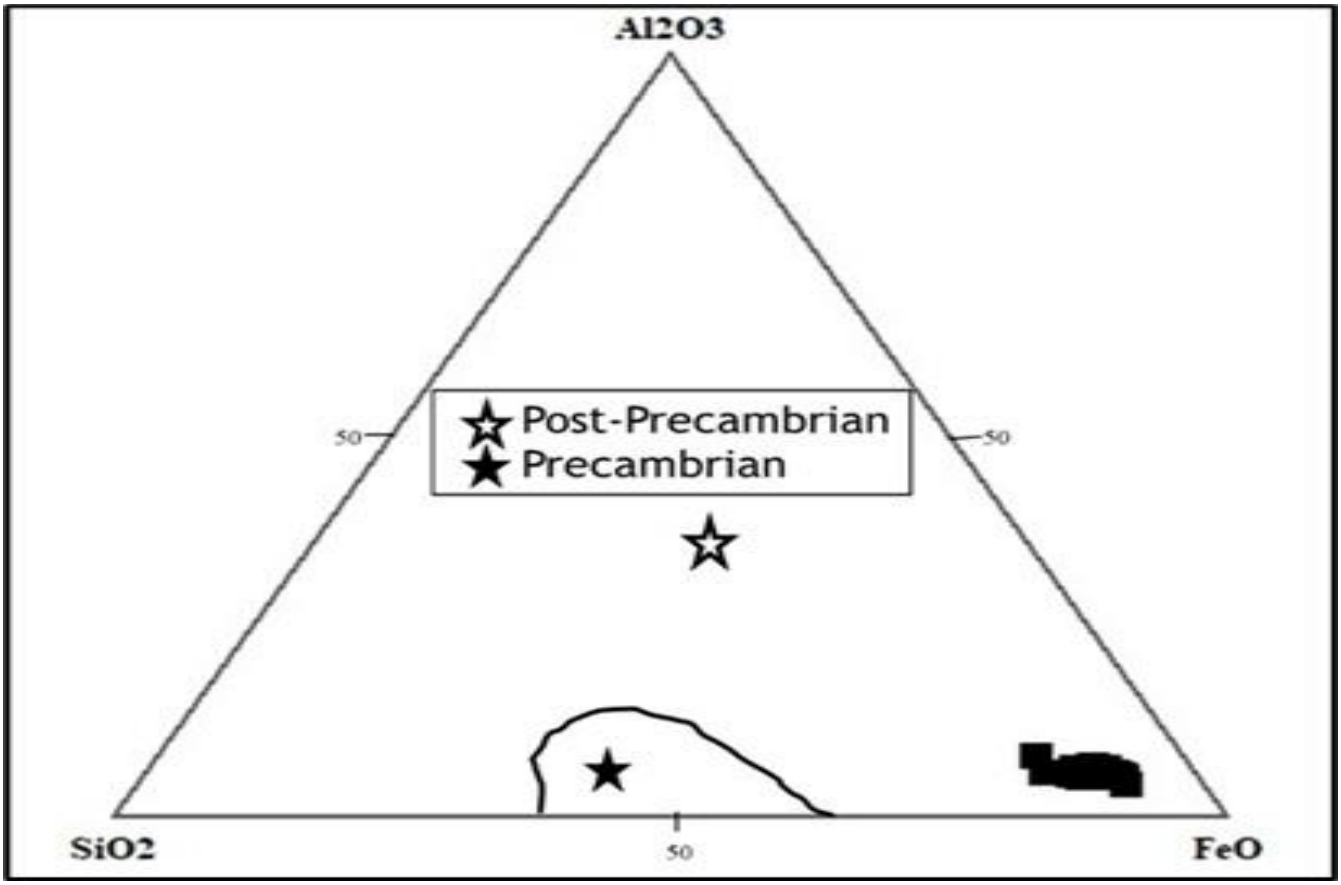

Fig. 3. SiO_2-Al_2O_3-FeO ternary diagram showing the post-Precambrian iron bearing metasediment in Mfamosing (field after Govett *et al.*, 1966)

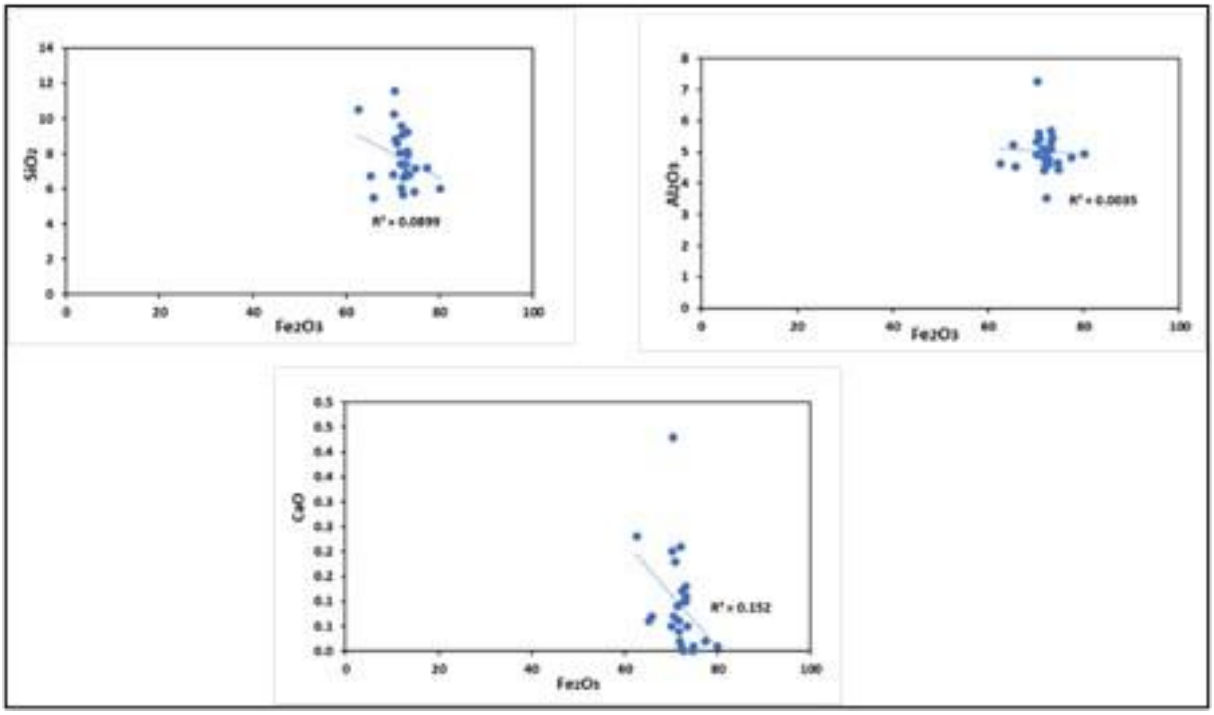

Fig. 4. Selected binary plots of major oxides against Fe_2O_3 for Mfamosing iron formation

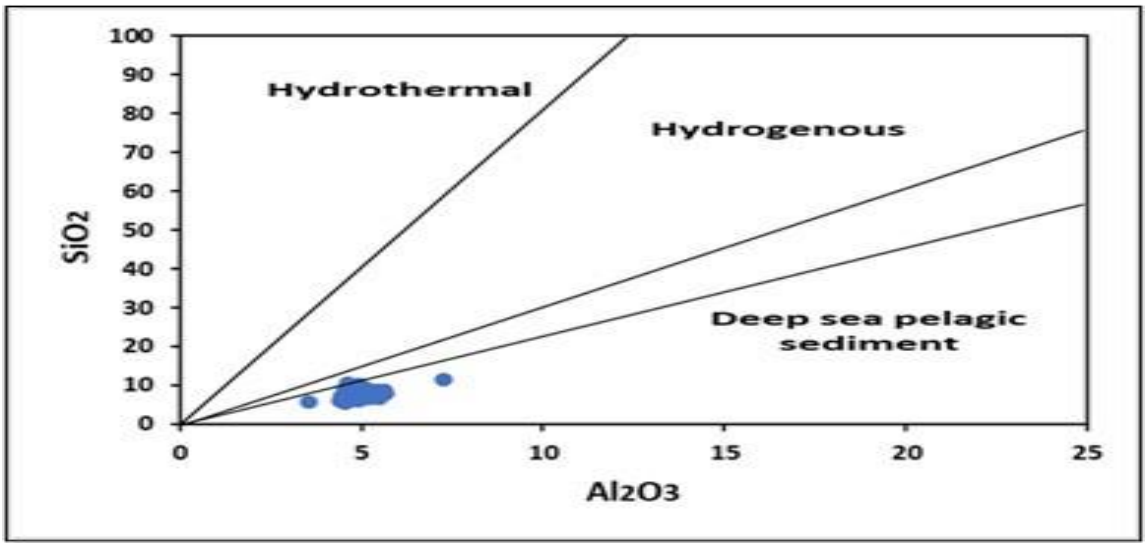

Fig. 5. SiO_2 - Al_2O_3 discrimination diagram indicating the deep-sea pelagic sediment of Mfamosing iron formation (Field after Bostrom et al., 1973)

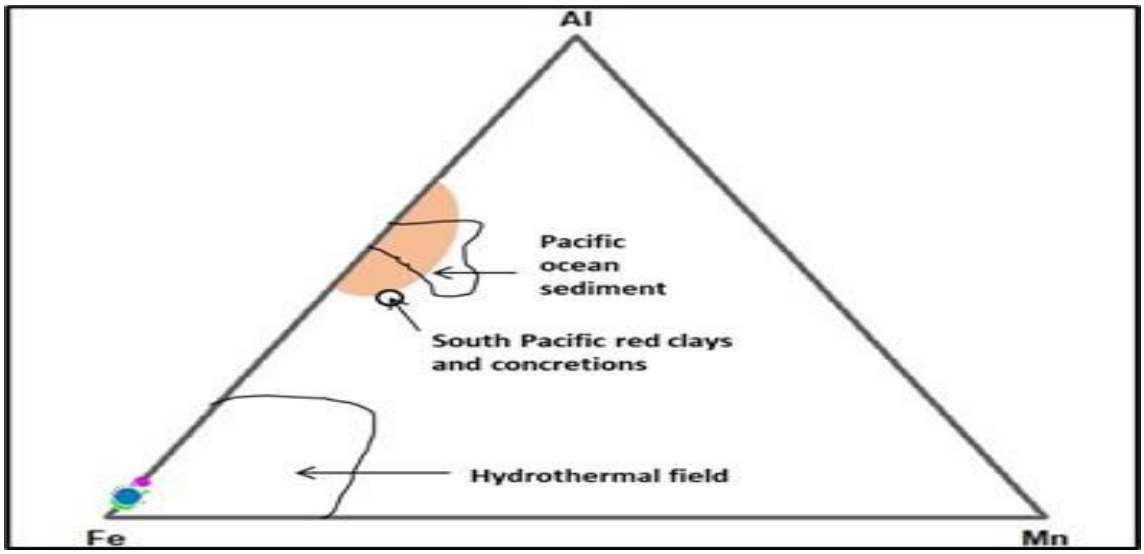

Fig. 6. Ternary Fe-Mn-Al plot showing hydrothermal affinity of Mfamosing iron formation (Field after Bonatti *et al.*, 1975)

3.3. Implication for Industrial Utilization

The geochemical analysis of iron ore samples from the Mfamosing areas not only sheds light on the ore's composition but also proves instrumental in evaluating its suitability for various industrial applications. According to the criteria proposed by Guider (1981) and Dobbins *et al*. (1982), commercial iron ore should ideally have tolerable concentrations of deleterious elements, with limits set at 0.07 wt-% for phosphorus (P) and 0.1 wt-% for sulfur (S) (Riposan *et al.*, 2013). The remarkably low concentrations of these deleterious elements in the analyzed samples indicate the ore's high quality, indicating that it is relatively free of impurities which is capable of adversely affecting industrial processes. Iron ores are conventionally classified into three categories, as outlined by Robinson *et al.* (2020): high-grade (Fe_2O_3 content above 65 wt-%), medium-grade (Fe_2O_3 concentration fluctuating between 52 and 65 wt-%), and low-grade (Fe_2O_3 values below 52 wt-%)(Angerer *et al.,* 2021). Most samples from the study area fall within the high-grade class, attesting to the exceptional iron content. This classification is supported by the whole-rock (MgO + CaO + MnO)/Fe_2O_3 total versus SiO_2/Fe_2O_3 total

discrimination diagram in Fig. 7, following the approach by Angerer *et al.* (2012).

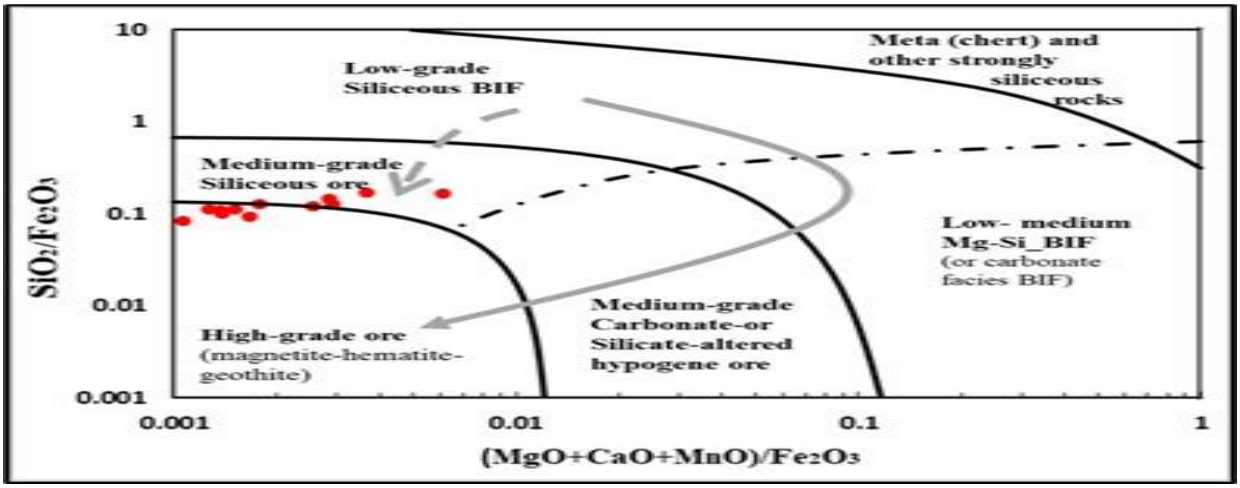

Fig. 7. Whole-rock (MgO + CaO + MnO)/Fe_2O_3 total versus SiO_2/Fe_2O_3 total discrimination diagram (Angerer *et al.*, 2012)

Comparative analysis with other iron formations in Nigeria, such as Gangfelum BIF, Maru BIF, Muro BIF, and Kankun BIF, revealing that the iron ore from the study area boasts higher iron content and a reduced presence of gangue minerals (Angerer *et al.*, 2022). Fig. 8, shows the spatial distribution of Mfamosing iron ore compared with Gangfelum BIF, Maru BIF, Muro BIF, and Kankun BIF. Similarly, when compared to international iron formations like Endergue BIF, Elom BIF, and Um Arab IF, the study area stands out with its superior iron content and minimal gangue minerals as outlined in Table 4.

Table 4. Comparison of the study area major oxides (wt-%) with IF and BIF types areas of the world (Robinson *et al.*, 2020)

Location	SiO_2	TiO_2	Al_2O_3	Fe_2O_3(t)	MnO	MgO	CaO	Na_2O	K_2O	P_2O_5
This Study	7.70	0.00	5.01	70.98	0.00	0.00	0.10	0.00	0.05	0.00
Endengue IF	36.77	0.19	1.95	56.29	0.10	0.77	0.16	0.0	0.07	0.07
Ngovayang IF	46.84	0.51	3.76	43.68	0.07	2.69	1.49	0.28	1.08	0.24
Elom BIF	39.98	0.03	0.48	58.19	0.07	0.06	0.02	0.01	0.02	0.08
Bikoula BIF	37.77	0.36	2.88	49.97	0.48	4.44	3.15	0.85	0.76	0.11
Nkout BIF	40.12	0.03	0.83	53.88	0.09	2.61	1.07	0.10	0.26	0.08
Um Anab (Egypt) IF	54.62	0.20	3.60	35.14	0.07	1.28	2.98	0.25	0.12	0.54
Jerome (USA) IF	18.16	0.04	1.04	77.78	0.13	0.09	0.92	0.09	0.22	/
Algoma BIF	50.50	/	3.00	41.33	0.22	1.53	1.51	0.31	0.58	0.21
Superior BIF	47.20	/	1.39	44.51	0.73	1.24	1.58	0.12	0.14	0.06

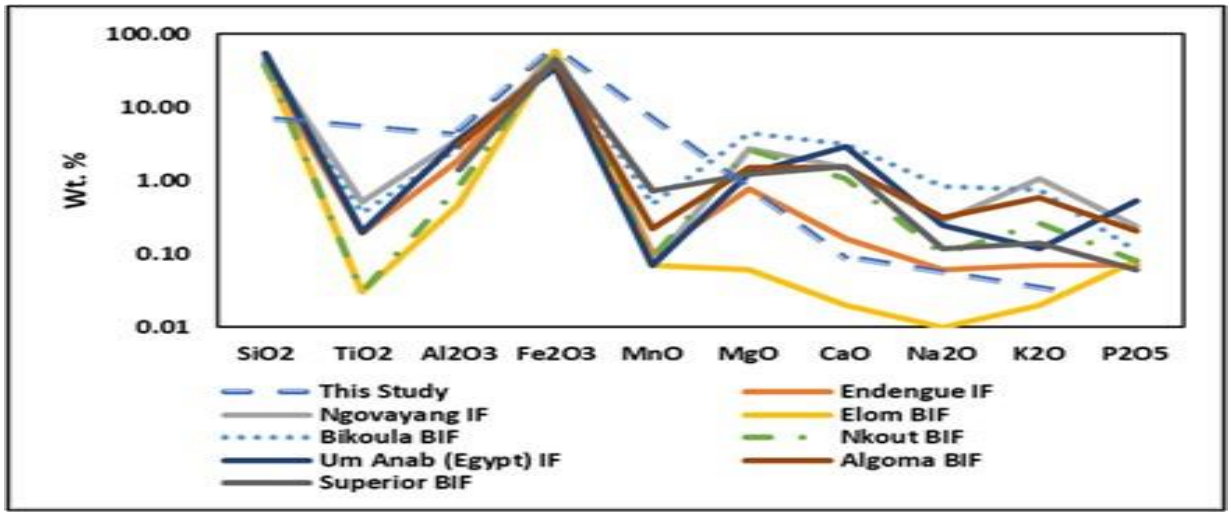

Fig. 8. Spider plot showing the variation of the study area major oxides (wt-%) with BIF types in Nigeria

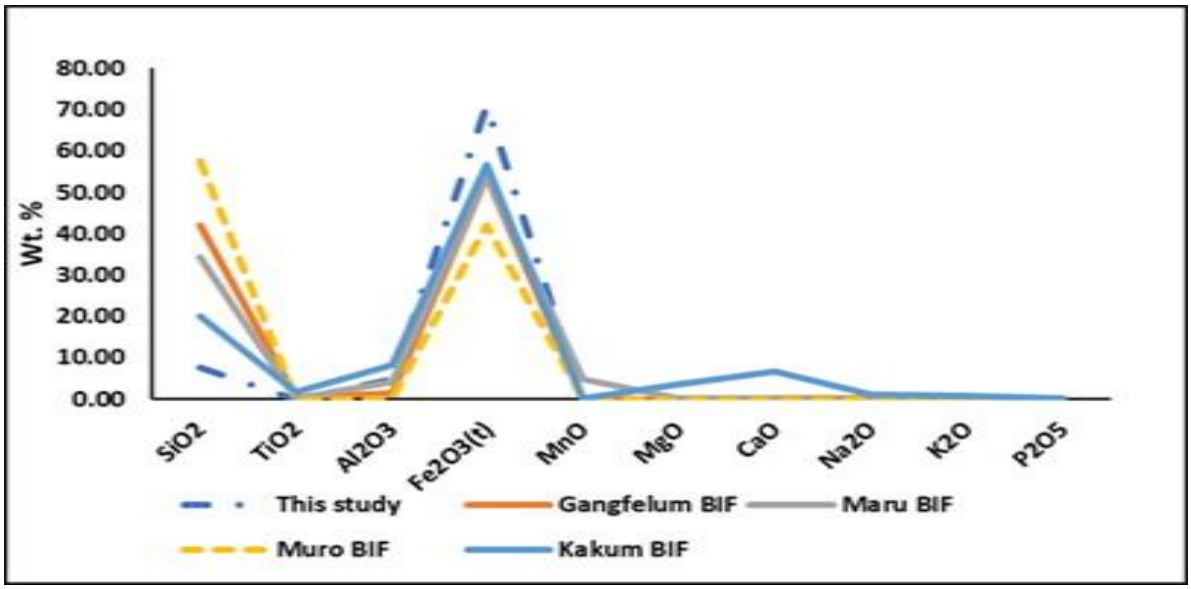

Fig. 9. Spider plot showing the variation of the study area major oxides (wt-%) with IF and BIF types areas of the world

The spatial distribution of Mfamosing iron ore compared with global data is shown in Fig. 9. The iron content of the Mfamosing iron ore is also competitive on a global scale, aligning with major productive iron formations worldwide, including Quadrilátero Ferrífero (Brazil), Carajás (Brazil), Hamersley (Australia), Krivoy Rog (Ukraine), Bailadila (India).Also, Steel, being one of the most versatile and crucial materials in the global economy, would benefit from the high-quality ore extracted from the Mfamosing region, positioning it as a valuable resource in the global industrial landscape.

4.0 Conclusion

The detailed analysis of the Mfamosing iron ore presents a compelling picture of a deposit distinguished by its remarkably high hematite content, averaging 70.98 wt.%. The coexistence of quartz and aluminosilicates as gangue minerals, coupled with minimal contamination from other oxides, underscores the ore's purity and uniqueness. The observed inverse correlations between Fe_2O_3 and SiO_2, Al_2O_3, and CaO suggest a potential chemical precipitation mechanism during ore formation, providing valuable insights into the geological processes shaping the deposit. Comparative analyses with other iron

formations highlight the economic significance of the Mfamosing deposit, emphasizing its exceptional iron content and distinctive composition globally. The ore's sedimentary origin is supported by the SiO_2-Al_2O_3-FeO ternary diagram, aligning with a post-Precambrian age. Hydrothermal influence, evidenced by high Fe/Al and Fe/Si ratios, further enhances the ore's richness and purity, emphasizing marine influence and minimal detrital material input. The ore's high quality, meeting industry standards for deleterious elements, classifies it as predominantly high-grade iron ore, making it a valuable resource for global steel production and cement industries. The Mfamosing iron ore stands out on both regional and international scales, positioning itself as a key contributor to the global industrial landscape.

5.0 Acknowledgement

The authors would like to acknowledge all the authors for their contribution to ensuring the successful completion of this research work. The authors also acknowledge Petters *et al.*, (2014), William *et al.*, (2019), Govett *et al.*, (1966), Bostrom *et al.*, (1973), Bonatti *et al.*, (1975), and Angerer *et al.*, (2012) whose works were instrumental in this research

6.0 References

Adamu, C. I., Omang, B. O., Oyetade, O. P., Johnson, O., & Nganje, T. N. (2021). Trace and rare earth element geochemistry of the black and grey shales of the Calabar flank, Southeastern Nigeria: constraints on the depositional environment and the degree of metal enrichment. *Acta Geochimica*, *40*, 312-324.

Adedeji, F. A., & Sale, F. R. (1984). Characterization and reducibility of Itakpe and Agbaja (Nigerian) iron ores. *Clay Minerals*, *19*(5), 843–856. https://doi.org/10.1180/claymin.1984.019.5.12

Adekoya, J. A. (1998). The geology and geochemistry of the Maru Banded Iron-Formation, northwestern Nigeria. *Journal of African Earth Sciences*, *27*(2), 241–257. https://doi.org/10.1016/S0899-5362(98)00059-1

Angerer, T., Thorne, W., Hagemann, S. G., Tribus, M., Evans, N. J., & Savard, D. (2022). Iron oxide chemistry supports a multistage hydrothermal genesis of BIF-hosted hematite ore in the Mt. Tom Price and Mt. Whaleback deposits. *Ore Geology Reviews*, *144*, 104840. https://doi.org/10.1016/j.oregeorev.2022.104840

Anoh, N. O., & Petters, S. W. (2014). Preliminary investigation of Late Turonian-Early Campanian shallow marine foraminifera of the Mungo River/Logbadjeck Formation, NW Douala Basin, Cameroon. *Journal of African Earth Sciences*, *99*, 442–451. https://doi.org/10.1016/j.jafrearsci.2013.11.003

Bafon, T. G., Bolarinwa, A. T., Suh, C. E., Oljira, T., Bedada, B. A., Ngoran, G. N., Ateh, K. I., Djoumbissie, B. M. K., & Ngang, C. T. (2023). Petrogenetic characterization of the host rocks of the Sanaga iron ore prospect, southern Cameroon. *Acta Geochimica*, *42*(2), 195–220. https://doi.org/10.1007/s11631-022-00574-7

Bekker, A., Planavsky, N. J., Krapež, B., Rasmussen, B., Hofmann, A., Slack, J. F., Rouxel, O. J., & Konhauser, K. O. (2014). Iron Formations: Their Origins and Implications for Ancient Seawater Chemistry. In *Treatise on Geochemistry* (pp. 561–628). Elsevier. https://doi.org/10.1016/B978-0-08-095975-7.00719-1

Bekker, A., Slack, J. F., Planavsky, N., Krapez, B., Hofmann, A., Konhauser, K. O., & Rouxel, O. J. (2010). Iron Formation: The Sedimentary Product of a Complex Interplay among Mantle, Tectonic, Oceanic, and Biospheric Processes. *Economic Geology*, *105*(3), 467–508. https://doi.org/10.2113/gsecongeo.105.3.467

Bolarinwa, A. T. (2017). Petrography and Geochemistry of the Banded Iron Formation of the Gangfelum Area, Northeastern Nigeria. *Earth Science Research*, *7*(1), 25. https://doi.org/10.5539/esr.v7n1p25

Clout, J. M. F., & Simonson, B. M. (2005). Precambrian Iron Formations and Iron Formation-Hosted Iron Ore Deposits. In J. W. Hedenquist, J. F. H. Thompson, R. J. Goldfarb, & J. P. Richards, *One Hundredth Anniversary Volume*. Society of Economic Geologists. https://doi.org/10.5382/AV100.20

Cox, G. M., Halverson, G. P., Minarik, W. G., Le Heron, D. P., Macdonald, F. A., Bellefroid, E. J., & Strauss, J. V. (2013). Neoproterozoic iron formation: An evaluation of its temporal, environmental and tectonic significance. *Chemical Geology*, *362*, 232–249. https://doi.org/10.1016/j.chemgeo.2013.08.002

Das, B., Prakash, S., Reddy, P. S. R., & Misra, V. N. (2007). An overview of utilization of slag and sludge from steel industries. *Resources, Conservation and Recycling*, *50*(1), 40–57. https://doi.org/10.1016/j.resconrec.2006.05.008

Edegbai, A. J., Schwark, L., & Oboh-Ikuenobe, F. E. (2019). A review of the latest Cenomanian to Maastrichtian geological evolution of Nigeria and its stratigraphic and paleogeographic implications. *Journal of African Earth Sciences*, *150*, 823–837. https://doi.org/10.1016/j.jafrearsci.2018.10.007

Ekwok, S. E., Akpan, A. E., & Ebong, E. D. (2019). Enhancement and modelling of aeromagnetic data of some inland basins, southeastern Nigeria. *Journal of African Earth Sciences*, *155*, 43–53. https://doi.org/10.1016/j.jafrearsci.2019.02.030

Ekwok, S. E., Akpan, A. E., & Ebong, E. D. (2021). Assessment of crustal structures by gravity and magnetic methods in the Calabar Flank and adjoining areas of Southeastern Nigeria—A case study. *Arabian Journal of Geosciences*, *14*(4), 308. https://doi.org/10.1007/s12517-021-06696-1

Fiege, J. L. (2019). *The formation of Kiruna-type iron oxide-apatite deposits: A new genetic model*. https://doi.org/10.15488/5496

Gourcerol, B., Thurston, P. C., Kontak, D. J., Côté-Mantha, O., & Biczok, J. (2016). Depositional setting of Algoma-type banded iron formation. *Precambrian Research*, *281*, 47–79. https://doi.org/10.1016/j.precamres.2016.04.019

Hagemann, S. G., Angerer, T., Duuring, P., Rosière, C. A., Figueiredo E Silva, R. C., Lobato, L., Hensler, A. S., & Walde, D. H. G. (2016). BIF-hosted iron mineral system: A review. *Ore Geology Reviews*, *76*, 317–359. https://doi.org/10.1016/j.oregeorev.2015.11.004

Harry, T. A. (2022). Upper-Cretaceous and Paleocene Biostratigraphy of Nkporo Shales, Calabar Flank, Southern Benue Trough. *Journal of Nature, Science & Technology*, *2*(1), 1–5. https://doi.org/10.36937/janset.2022.6572

Hussin, A., Rahman, A. H. A., & Ibrahim, K. Z. (2018). Mineralogy and geochemistry of clays from Malaysia and its industrial application. *IOP Conference Series: Earth and Environmental Science*, *212*, 012040. https://doi.org/10.1088/1755-1315/212/1/012040

Jansson, N. F., & Allen, R. L. (2011). The origin of skarn beds, Ryllshyttan Zn–Pb–Ag + magnetite deposit, Bergslagen, Sweden. *Mineralogy and Petrology*, *103*(1–4), 49–78. https://doi.org/10.1007/s00710-011-0154-x

Jean-Lavenir, N. M., Cyrille, S., Cedric, D. M., Estelle, N. E. T. P., Mukete, C. D., & Gloire, K. T. S. (2023). *Petrogenetic Characterization of Banded Iron Formations of Bidjouka Area, Nyong Complex, Southern Cameroon: Implication for the Origin and Depositional Environment of Paleoproterozic Bifs* [Preprint]. SSRN. https://doi.org/10.2139/ssrn.4492338

Kimberley, M. M. (1978). Paleoenvironmental classification of iron formations. *Economic Geology*, *73*(2), 215–229. https://doi.org/10.2113/gsecongeo.73.2.215

Konhauser, K. O., Planavsky, N. J., Hardisty, D. S., Robbins, L. J., Warchola, T. J., Haugaard, R., Lalonde, S. V., Partin, C. A., Oonk, P. B. H., Tsikos, H., Lyons, T. W., Bekker, A., & Johnson, C. M. (2017). Iron formations: A global record of Neoarchaean to Palaeoproterozoic environmental history. *Earth-Science Reviews*, *172*, 140–177. https://doi.org/10.1016/j.earscirev.2017.06.012

Li, F., Zhu, X., Ding, H., & Zhang, K. (2022). Local hydrothermal sources for Superior-type iron formations: Insights from the Animikie Basin. *Precambrian Research*, *377*, 106736. https://doi.org/10.1016/j.precamres.2022.106736

Liu, B., Zhang, Y., Lu, M., Su, Z., Li, G., & Jiang, T. (2019). Extraction and separation of manganese and iron from ferruginous manganese ores: A review. *Minerals Engineering*, *131*, 286–303. https://doi.org/10.1016/j.mineng.2018.11.016

Madondo, J., Canet, C., Núñez-Useche, F., & González-Partida, E. (2021). Geology and geochemistry of jasperoids from the 'Montaña de Manganeso' district, San Luis Potosí, north-central Mexico. *Revista Mexicana de Ciencias Geológicas*, *38*(3), 193–209. https://doi.org/10.22201/cgeo.20072902e.2021.3.1651

Marion, K. W. M., Djibril, K. N. G., Guimollaire, N. D., & Patrick, A. K. (2021). Petrogenesis and U–Pb zircon dating of amphibolite in the Mewengo iron deposit, Nyong series, Cameroon: Fingerprints of iron depositional geotectonic setting. *Arabian Journal of Geosciences*, *14*(10), 872. https://doi.org/10.1007/s12517-021-07235-8

Minitti, M. E., Lane, M. D., & Bishop, J. L. (2005). A new hematite formation mechanism for Mars. *Meteoritics & Planetary Science*, *40*(1), 55–69. https://doi.org/10.1111/j.1945-5100.2005.tb00364.x

Moisescu, C., Ardelean, I. I., & Benning, L. G. (2014). The effect and role of environmental conditions on magnetosome synthesis. *Frontiers in Microbiology*, *5*. https://doi.org/10.3389/fmicb.2014.00049

Nanda, S. K., & Beura, D. (2021). Implicating the Origin and Depositional Environment of Banded Iron Formation (BIF) of Bonai-Keonjhar Iron Ore Belt in Eastern India from its Petrography and Geochemistry. *Geology of Ore Deposits*, *63*(6), 497–514. https://doi.org/10.1134/S1075701521060076

Ndime, E. N., Ganno, S., Soh Tamehe, L., & Nzenti, J. P. (2018). Petrography, lithostratigraphy and major element geochemistry of Mesoarchean metamorphosed banded iron formation-hosted Nkout iron ore deposit, north western Congo craton, Central West Africa. *Journal of African Earth Sciences*, *148*, 80–98. https://doi.org/10.1016/j.jafrearsci.2018.06.007

Nkuna, R., Ijoma, G. N., Matambo, T. S., & Chimwani, N. (2022). Accessing Metals from Low-Grade Ores and the Environmental Impact Considerations: A Review of the Perspectives of Conventional versus Bioleaching Strategies. *Minerals*, *12*(5), 506. https://doi.org/10.3390/min12050506

Ochromowicz, K., Aasly, K., & Kowalczuk, P. (2021). Recent Advancements in Metallurgical Processing of Marine Minerals. *Minerals*, *11*(12), 1437. https://doi.org/10.3390/min11121437

Okon, E. E., Kudamnya, E. A., Oyeyemi, K. D., Omang, B. O., Ojo, O., & Metwaly, M. (2022). Field Observations and Geophysical Research Applied to the Detection of Manganese (Mn) Deposits in the Eastern Part of Oban Massif, South-Eastern Nigeria: An Integrated Approach. *Minerals*, *12*(10), 1250.

Omang, B.O., Effiom, H., Omeka, E., Oko, E., Asinya, A., Ojikutu, T., & Kave, T. (2023). Trace element geochemical imprints and multi-path health risk assessment of potentially toxic elements in soils from the polymetallic area of tashan-jatau, northwestern nigeria. *Global*

Journal of Geological Sciences, 21(1), 91-115

Omang B.O, Asinya E.A, Udinmwen E, Oyetade O.P: Structural framework and deformation episodes in the Igarra schist belt southwestern Nigeria. *Global Journal of Geological Sciences vol20(1),1-17 2022 DOI: 10.4314/gjgs.v20i1.1*

Omang, B. O., Omeka, M. E., Asinya, E. A., Oko, P. E., & Aluma, V. C. (2023). Application of GIS and feedforward back-propagated ANN models for predicting the ecological and health risk of potentially toxic elements in soils in Northwestern Nigeria. *Environmental Geochemistry and Health*, 1-33

Omietimi, E., Lenhardt, N., & Bumby, A. (2022). *Sedimentology, paleoclimate proxy, paleoenvironment proxies* (p. 145295 Bytes) [dataset]. University of Pretoria. https://doi.org/10.25403/UPRESEARCHDATA.21510903.V1

Omotunde, V. B. (2020). Mineralogy and Geochemistry of Hydrothermally altered Talcose rocks from Ila Orangun-Oyan areas, part of Southwestern Nigeria. *Indian Journal of Science and Technology*, *13*(40), 4244–4261. https://doi.org/10.17485/IJST/v13i40.1686

Öztürk, H., Kasapçı, C., Cansu, Z., & Hanilçi, N. (2016). Geochemical characteristics of iron ore deposits in central eastern Turkey: An approach to their genesis. *International Geology Review*, *58*(13), 1673–1690. https://doi.org/10.1080/00206814.2016.1183236

Planavsky, N., Rouxel, O. J., Bekker, A., Hofmann, A., Little, C. T. S., & Lyons, T. W. (2012). Iron isotope composition of some Archean and Proterozoic iron formations. *Geochimica et Cosmochimica Acta*, *80*, 158–169. https://doi.org/10.1016/j.gca.2011.12.001

Posth, N. R., Canfield, D. E., & Kappler, A. (2014). Biogenic Fe(III) minerals: From formation to diagenesis and preservation in the rock record. *Earth-Science Reviews*, *135*, 103–121. https://doi.org/10.1016/j.earscirev.2014.03.012

Reddy, K. R., Gopakumar, A., & Chetri, J. K. (2019). Critical review of applications of iron and steel slags for carbon sequestration and environmental remediation. *Reviews in Environmental Science and Bio/Technology*, *18*(1), 127–152. https://doi.org/10.1007/s11157-018-09490-w

Riposan, I., Chisamera, M., & Stan, S. (2013). Control of Surface Graphite Degeneration in Ductile Iron for Windmill Applications. *International Journal of Metalcasting*, *7*(1), 9–20. https://doi.org/10.1007/BF03355540

Rojas, P. A., Barra, F., Deditius, A., Reich, M., Simon, A., Roberts, M., & Rojo, M. (2018). New contributions to the understanding of Kiruna-type iron oxide-apatite deposits revealed by magnetite ore and gangue mineral geochemistry at the El Romeral deposit, Chile. *Ore Geology Reviews*, *93*, 413–435. https://doi.org/10.1016/j.oregeorev.2018.01.003

Santoro, L., Putzolu, F., Mondillo, N., Boni, M., & Herrington, R. (2022). Trace element geochemistry of iron-(oxy)-hydroxides in Ni(Co)-laterites: Review, new data and implications for ore forming processes. *Ore Geology Reviews*, *140*, 104501. https://doi.org/10.1016/j.oregeorev.2021.104501

Skirrow, R. G. (2022). Iron oxide copper-gold (IOCG) deposits – A review (part 1): Settings, mineralogy, ore geochemistry and classification. *Ore Geology Reviews*, *140*, 104569. https://doi.org/10.1016/j.oregeorev.2021.104569

Sun, S., & Li, Y.-L. (2017). Geneses and evolutions of iron-bearing minerals in banded iron formations of >3760 to ca. 2200 million-year-old: Constraints from electron microscopic, X-ray diffraction and Mössbauer spectroscopic investigations. *Precambrian Research*, *289*, 1–17. https://doi.org/10.1016/j.precamres.2016.11.010

Taner, M. F., & Chemam, M. (2015). Algoma-type banded iron formation (BIF), Abitibi Greenstone belt, Quebec, Canada. *Ore Geology Reviews*, *70*, 31–46. https://doi.org/10.1016/j.oregeorev.2015.03.016

Tchouakui, R. D. K., Soh Tamehe, L., Ganno, S., Nzepang Tankwa, M., & Nzenti, J. P. (2022). Petrography and geochemistry of the Moloundou pelite–chert complex and high-grade iron ore, southeast Cameroon: Implications for provenance and tectonic setting. *Arabian Journal of Geosciences*, *15*(23), 1731. https://doi.org/10.1007/s12517-022-10981-y

Teutsong, T., Temga, J. P., Enyegue, A. A., Feuwo, N. N., & Bitom, D. (2021). Petrographic and geochemical characterization of weathered materials developed on BIF from the Mamelles iron ore deposit in the Nyong unit, South-West Cameroon. *Acta Geochimica*, *40*(2), 163–175. https://doi.org/10.1007/s11631-020-00421-7

Thomas Angerer, Hagemann, S. G., & Walde, D. H. G. (2021). Diagenetic and supergene ore forming processes in the iron formation of the Neoproterozoic Jacadigo Group, Corumbá, Brazil. *Journal of South American Earth Sciences*, *105*, 102902. https://doi.org/10.1016/j.jsames.2020.102902

Thombare, N., Jha, U., Mishra, S., & Siddiqui, M. Z. (2016). Guar gum as a promising starting material for diverse applications: A review. *International Journal of Biological Macromolecules*, *88*, 361–372. https://doi.org/10.1016/j.ijbiomac.2016.04.001

Uzoegbu, M. U., Obaje, N. G., & Omang, B. O. (2023). Pyrolytic and provenance evaluation of organic matter from the tertiary niger delta basin, nigeria: implication on hydrocarbon generation. *Global Journal of Geological Sciences*, 21(1), 51-67

Vishiti, A.; Suh, C.E.; Ngatcha, R.B.; Melchiorre, E.B.; Shemang, E.M.; Omang, B.O.; Ngang, T.C.; Valdez, F.C.; Sekem, S.G. Soil Geochemistry Combined with Particulate Gold Microchemistry Provides Evidence of Eluvial Gold Genesis and Anthropogenic Hg Use in Eastern Cameroon Goldfields. Minerals 2024, 14, 567. hps://doi.org/10.3390/min14060567

Vural, A. (2023). An evaluation of elemental enrichment in rocks: In the case of Kısacık and its neighborhood (Ayvacık, Çanakkale/Türkiye). *Journal of Geography and Cartography*, *6*(1), 1850. https://doi.org/10.24294/jgc.v6i1.1850

Wang, C., Zhang, L., Lan, C., & Dai, Y. (2014). Petrology and geochemistry of the Wangjiazhuang banded iron formation and associated supracrustal rocks from the Wutai greenstone belt in the North China Craton: Implications for their origin and tectonic setting. *Precambrian Research*, *255*, 603–626. https://doi.org/10.1016/j.precamres.2014.08.002

Xing, Y., Brugger, J., Etschmann, B., Tomkins, A. G., Frierdich, A. J., & Fang, X. (2021). Trace element catalyses mineral replacement reactions and facilitates ore formation. *Nature Communications*, *12*(1), 1388. https://doi.org/10.1038/s41467-021-21684-5

Yang, X., Zhang, Z., Guo, S., Chen, J., & Wang, D. (2016). Geochronological and geochemical studies of the metasedimentary rocks and diabase from the Jingtieshan deposit, North Qilian, NW China: Constraints on the associated banded iron formations. *Ore Geology Reviews*, *73*, 42–58. https://doi.org/10.1016/j.oregeorev.2015.10.018

Yin, J., Li, H., & Xiao, K. (2023). Origin of Banded Iron Formations: Links with Paleoclimate, Paleoenvironment, and Major Geological Processes. *Minerals*, *13*(4), 547. https://doi.org/10.3390/min13040547

Zhang, Z., Hou, T., Santosh, M., Li, H., Li, J., Zhang, Z., Song, X., & Wang, M. (2014). Spatio-temporal distribution and tectonic settings of the major iron deposits in China: An overview. *Ore Geology*

Reviews, 57, 247–263. https://doi.org/10.1016/j.oregeorev.2013.08.021.

Compliance with Ethical Standards Declaration

Ethical Approval

Not Applicable

Competing interests

The authors declare that they have no known competing financial interests

Funding

The authors declared no external source of funding.

Availability of data and materials

Data would be made available on request**.**

Authors' contributions

Benjamin Odey Omang: Project conceptualization, supervision and mauscript second draft**.** Temple Okah Arikpo: Data extraction and analysis. Eyong Gods'will Abam: ploting and interpretation of plots. Asinya Enah Asinya: Manuscript first draft Godwin Terwase Kave: Manuscript proofreading. Anthony Adesoji Onansonwo: Revision